Activation of Photocatalytic Water Oxidation on N-Doped ZnO Bundle-like Nanoparticles under Visible Light

ARTICLE *in* THE JOURNAL OF PHYSICAL CHEMISTRY C · MARCH 2013

Impact Factor: 4.77 · DOI: 10.1021/jp311729b

9 AUTHORS, INCLUDING:

Zhi-Gang Chen
University of Queensland
137 PUBLICATIONS **4,692** CITATIONS
SEE PROFILE

Zheng Xing
Monash University (Australia)
11 PUBLICATIONS **120** CITATIONS
SEE PROFILE

Lianzhou Wang
University of Queensland
217 PUBLICATIONS **5,346** CITATIONS
SEE PROFILE

THE JOURNAL OF PHYSICAL CHEMISTRY C

Article

pubs.acs.org/JPCC

Activation of Photocatalytic Water Oxidation on N-Doped ZnO Bundle-like Nanoparticles under Visible Light

Xu Zong,[†] Chenghua Sun,[†] Hua Yu,[†] Zhi Gang Chen,[‡] Zheng Xing,[†] Delai Ye,[†] Gao Qing (Max) Lu,[†] Xinyong Li,[§] and Lianzhou Wang*[,†]

[†]ARC Centre of Excellence for Functional Nanomaterials, School of Chemical Engineering and AIBN, The University of Queensland, QLD 4072, Australia

[‡]Materials Engineering, The University of Queensland, QLD 4072, Australia

[§]Key Laboratory of Industrial Ecology and Environmental Engineering (MOE) and State Key Laboratory of Fine Chemical, School of Environmental Science and Technology, Dalian University of Technology, Dalian 116024, China

Supporting Information

ABSTRACT: Nitrogen-doped ZnO bundle-like nanoparticles were prepared by heating ZnOHF precursor at different temperatures under an ammonia atmosphere. ZnOHF gradually transformed to N-ZnO with the increase of the heating temperature, and the as-prepared N-ZnO nanoparticles preserved the original morphologies of ZnOHF at moderate heating temperature. The N-ZnO nanoparticles demonstrated drastically enhanced absorption in the visible region compared with the commercial ZnO and N-ZnO derived from commercial ZnO. Theoretical calculations indicated that the contribution of nitrogen to the top of the valence band (VB) of ZnO plays the major role of extending the absorption of ZnO to the visible region. The as-prepared N-ZnO showed high photocatalytic activity for the visible-light-induced water oxidation, and the activity can be further greatly enhanced by loading IrO_2 cocatalyst. To our knowledge, this is the first report of realizing photocatalytic water oxidation on non-metal-doped ZnO under visible light without applied bias, thus adding new value to the band gap engineering of benchmark ZnO for efficient solar energy utilization.

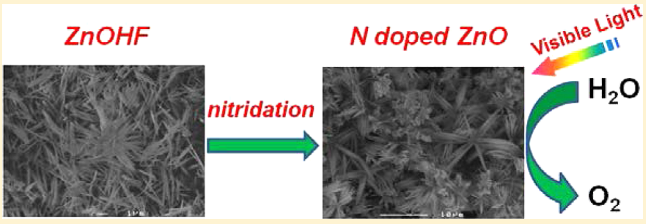

1. INTRODUCTION

Photocatalytic splitting of water with semiconductor materials represents an attractive approach toward the conversion of solar energy.[1−3] As a key component in the scheme of solar energy conversion, photocatalyst has been the focus of investigation. The development of new semiconductor materials or rational modification of existent ones has been continuously pursued.[4−6] In this regard, ZnO has been extensively studied due to its fascinating features such as nontoxicity, low cost, and high efficiency.[7−10] Especially compared with TiO_2, ZnO has a direct band gap, 10−100 times higher electron mobility, and correspondingly a reduced electrical resistance and enhanced electron transfer efficiency.[11] Therefore, ZnO is expected to be a good candidate for photocatalytic and photoelectrochemical applications. However, like TiO_2, ZnO has a wide band gap of 3.2 eV, which severely impairs the utilization of visible light accounting for 43% of the solar spectrum. To better utilize the solar energy, it is highly desirable to modify ZnO toward visible light response.

Metal and non-metal doping in semiconductors are the two general strategies to modify UV-responsive photocatalyst toward visible light response.[12,13] In particular, due to the compatible size to oxygen and small formation energy required for the substitution of O, N has been widely used as the dopant to modify the electronic structures of oxide semiconductors.[12] In this regard, N doping has been also applied to ZnO with the expectation of improving the light absorption property of ZnO in the visible region.[11,14−21] However, most efforts on N-doped ZnO (refer to N-ZnO hereafter) have been focused on N-ZnO films and their photoelectrochemical performance under applied bias,[14−18] while there are only few reports on the N-ZnO powders which are more favorable for direct applications in simple particulate aqueous system.[11,19−21] More importantly, unlike the widely studied N-TiO_2 counterpart, N-ZnO did not show appreciable photocatalytic performance (such as dye degradation) in the visible region as expected,[11,19] therefore making the efficacy of nitrogen doping on ZnO for photocatalysis suspicious.

Herein we demonstrated that nitrogen doping in ZnO bundle-like nanoparticles can lead to considerable absorption in the visible region and high performance for photocatalytic water oxidation under visible light. To our knowledge, this is the first report of realizing photocatalytic water oxidation on non-metal-doped ZnO under visible light without applied

Received: November 28, 2012
Revised: February 7, 2013
Published: February 21, 2013

external bias, thus adding new value to the band gap engineering of benchmark ZnO for efficient solar energy utilization.

2. EXPERIMENTAL SECTION

2.1. Preparation of Samples. ZnOHF nanobundles were first prepared according to a reported procedure and used as the precursor for the preparation of N-doped ZnO.[22] In a typical synthesis, 50 mL of $Zn(Ac)_2{\cdot}2H_2O$ (2 M), 100 mL of NaF(0.5 M), and 50 mL of hexamethylenetetramine (2 M) aqueous solution were added in sequence to a 1000 mL bottle containing 700 mL of deionized water. Upon the addition of hexamethylenetetramine, the mixed solution turned milky and the milky gel was stirred for 30 min. The bottle was then sealed and heated in an oven at 343 K for 5.5 h. After the completion of the reaction, the reaction solution was allowed to cool down to the room temperature. The resulting white precipitate was washed with deionized water and ethanol twice and then dried at 373 K for 12 h. N-doped ZnO was prepared by heating ZnOHF powders in NH_3 gas flow at temperatures from 673 to 1073 K for 5 h. After the nitridation reaction, the as-prepared product was allowed to cool down to the room temperature in NH_3 gas flow. To load IrO_2 (1.0 wt %) cocatalyst on N-ZnO, N-ZnO was impregnated with the appropriate amount of $Na_2IrCl_6{\cdot}6H_2O$ aqueous solution, followed by a heat treatment in Ar at 573 K for 1 h. N-doped TiO_2 was also prepared by heating TiO_2 in NH_3 gas flow at 873 K for 5 h.

2.2. Characterizations. X-ray diffraction (XRD) patterns of all samples were collected using a Bruker D8 advance X-ray diffractometer (Cu Kα radiation, λ = 1.5406 Å). The UV−vis absorption spectra for the samples were obtained on an UV−vis spectrophotometer (UV-2200, Shimadzu). X-ray photoelectron spectroscopy (XPS) was recorded with an X-ray photoelectron spectrometer (Thermo Escalab 250, a monochromatic Al KR X-ray source). The morphologies of N-doped ZnO were characterized with scanning electron microscopy (JEOL 6300) and transmission electron microscopy (TEM, Philips Tecnei F20).

2.3. Photocatalytic Reactions. The photocatalytic reactions were carried out in a quartz reaction cell connected to a closed gas circulation and evacuation system. 0.1 g of catalyst was suspended in 300 mL of aqueous solution containing $AgNO_3$ (0.01 M) and La_2O_3 (0.3 g). The suspension was then thoroughly degassed and irradiated by a 300 W Xe lamp (Beijing Trusttech Co. Ltd., PLS-SXE-300UV). The Xe lamp was equipped with an optical cutoff filter (λ > 420 nm) to eliminate ultraviolet light, and the reactor was equipped with a water filter to remove infrared light. The temperature of the reactant solution was maintained at 293 ± 5 K by a flow of cooling water during the reaction. The amount of O_2 produced was analyzed using an online gas chromatograph (GC-2014, Shimazu).

2.4. Photoelectrochemical Measurement. The N-ZnO electrodes were fabricated by coating viscous slurry of the N-ZnO powder on an FTO substrate with a screen-printing method. The FTO substrates were cleaned in advance by ultrasonication in acetone, ethanol, and distilled water and then dried with flowing nitrogen. The slurry consists of appropriate amounts of N-ZnO powder, terpineol, ethyl cellulose, and ethanol. The coating area of the electrode is about 1.6 cm^2. After coating the slurry on the FTO substrate, the slide was heated at 573 K in Ar for 1 h. Photoelectrochemical experiments were performed in a three-electrode cell made of quartz. A Pt wire, Ag/AgCl electrode, and N-ZnO electrodes were used as the counter, reference, and working electrodes, respectively. 0.1 M Na_2SO_4 solution continuously purged with Ar was used as the electrolyte. The CV measurements were performed at applied potential from −0.4 to +0.8 V with a scan rate of 20 mV/s. A 300 W Xe lamp (Beijing Trusttech Co. Ltd., PLS-SXE-300UV) was used as the light source for measurement. Current−voltage curves were taken on an electrochemical workstation (CHI660).

2.5. Theoretical Calculations. All calculations have been carried out using the density functional theory (DFT) within the generalized-gradient approximation (GGA),[23] with the exchange-correlation functional of Perdew−Burke−Ernzerhof (PBE).[24,25] This has been implemented in the Vienna ab initio simulation package (VASP),[26,27] which spans reciprocal space with a plane-wave basis, in this case up to a kinetic energy cutoff of 550 eV. To get better description of band gap narrowing, the on-site electron correlation is particularly necessary;[28−30] hence, DFT plus Hubbard model [DFT +U][28] is employed in our calculations. Following early publications,[31,32] U = 8.5 eV has been employed, which results in a partial correction to the band gap. In principle, the exact experimental value of band gap can be regenerated using bigger U values (e.g., 43.5 eV[33]); however, such big U values are physically unreasonable. In our calculation, the ZnO lattice is modeled by a supercell of 3 × 3 × 3 (dimensions: 9.75 Å × 9.75 Å × 15.62 Å), and k-space is sampled by a Monkhorst−Pack mesh of 3 × 3 × 3. N doping is modeled by replacing two oxygen atoms by nitrogen, leading to a doping ratio of 2/54.

3. RESULTS AND DISCUSSION

3.1. Characterization. In our typical sample synthesis, N-ZnO was prepared by ZnOHF precursor at elevated temperatures from 673 to 1073 K under NH_3 gas flow. After the heat treatment, bright yellow powder was observed on the quartz boat, and a small amount of black material was found on the outlet surface of the heating tube which is due to the volatilization of Zn element in a reductive atmosphere. Figure 1 shows the typical X-ray diffraction (XRD) patterns of the ZnOHF precursor, N-ZnO samples, and commercial ZnO. It was found that the diffraction peaks of all the N-ZnO samples prepared at a temperature higher than 873 K can be indexed to ZnO with hexagonal wurtzite structure. However, a heat

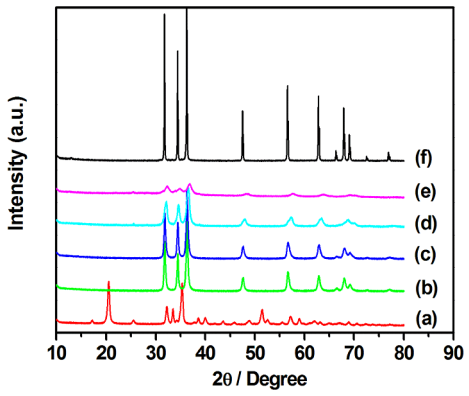

Figure 1. X-ray diffraction patterns of (a) ZnOHF precursor, (b−d) N-ZnO samples prepared by heating ZnOHF in NH_3 gas flow at 873, 973, and 1073 K for 2 h, (e) N-ZnO samples prepared by heating ZnOHF in NH_3 gas flow at 1073 K for 10 h, and (f) commercial ZnO.

dx.doi.org/10.1021/jp311729b | J. Phys. Chem. C 2013, 117, 4937−4942

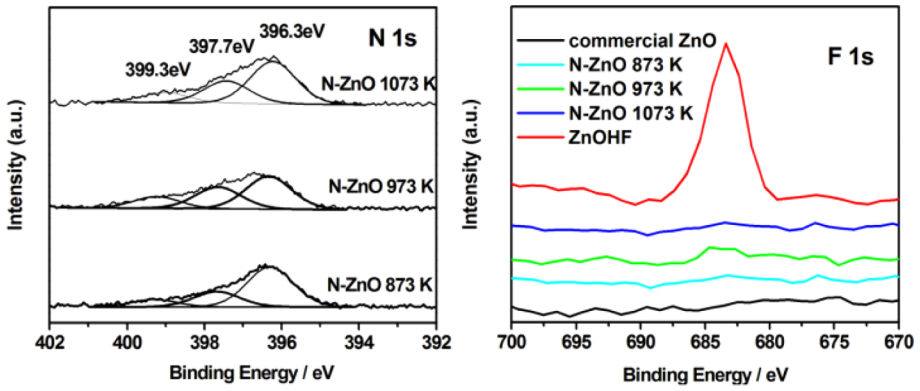

Figure 2. High-resolution XPS spectra of N 1s and F 1s measured on N-ZnO samples prepared by heating ZnOHF in NH_3 gas flow at different temperatures for 2 h.

treatment at temperature lower than 773 K can only produce a mixture of ZnO and ZnOHF (data not shown), indicating a gradual transformation from ZnOHF to ZnO during the heating treatment. A significant peak broadening and attenuation with the increase of the heating temperature and time was also observed, implying a decreasing crystallinity due to the incorporation of nitrogen into the ZnO. Moreover, the diffraction peak positions for N-ZnO are located at slightly higher angles than those for ZnO, suggesting an overall contraction of the lattice parameters (Figure S1, Supporting Information).

The chemical states of N, Zn, and O species in the as-prepared samples were then investigated by X-ray photoelectron spectroscopy (XPS) (Figure 2 and Figure S2). No signal for N species was observed for ZnO and ZnOHF. After heating ZnOHF in NH_3 flow, an asymmetric broad peak corresponding to the N species was observed, suggesting that more than one chemical state of N is present. The peak centered at 396.3 eV was attributed to the typical Zn−N bonds.[34] The peak of 399.2 eV is a typical value of the N 1s binding energy in amines.[35,36] The peak of 397.6 eV lies in between the typical binding energy found for zinc nitride (~396−397 eV)[37] and NO type species (above 400 eV)[38] and can be attributed to the N 1s of oxynitride (O−Zn−N).[37,39] Therefore, N is successfully doped at the O sites of ZnO during the nitridation reaction from ZnOHF precursor. In the previous work,[3] we successfully obtained F and N codoped TiO_2 by heating $TiOF_2$ precursor in flowing ammonia. However, contrary to what we have expected, no signals indexed to F were observed for the present N-ZnO samples even the sample were prepared with ZnOHF precursor. It was reported that ZnOHF will be decomposed into ZnO and HF during high-temperature treatment.[40] In our case, it is reasonable to suppose that ZnOHF will first decompose to form ZnO and HF during the heat treatment in NH_3 gas flow. The ZnO intermediate is subsequently doped with N, while HF reacts with NH_3 gas to form white NH_4F flake-like byproduct deposited on the downstream surface of the tube furnace (observed). As a result, N-ZnO can be successfully prepared from the ZnOHF precursor under a flowing NH_3 atmosphere.

The absorption properties of the resultant N-ZnO samples were then investigated with UV−vis diffuse reflectance spectroscopy (Figure 3). White commercial ZnO has an absorption cutoff edge at 375 nm, corresponding to a band gap of 3.3 eV. After heating commercial ZnO in NH_3, the as-obtained pale yellow N-ZnO exhibited an additional tail-like

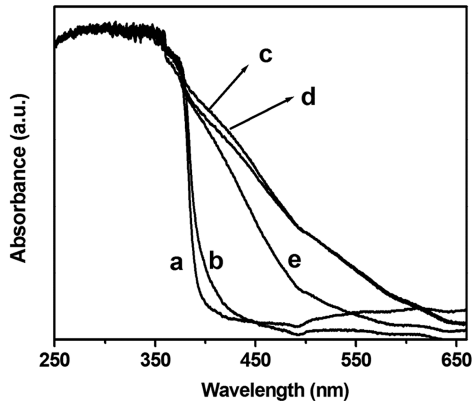

Figure 3. Diffuse reflectance spectra of (a) commercial ZnO, (b) N-ZnO prepared by nitriding commercial ZnO in NH_3 gas flow at 973 K for 5 h, and (c−e) N-ZnO prepared by heating ZnOHF in NH_3 gas flow at (c) 873 K, (d) 973 K, and (e) 1073 K for 2 h.

absorption in the visible region. However, the N-ZnO samples derived from ZnOHF exhibited a much stronger and broader absorption in the range from 420 to 650 nm, indicating an even notable modification of the band structure of ZnO derived from ZnOHF precursor. The remarkable influence of N-doping on the electronic structure of ZnO was clearly demonstrated by density functional theory calculations (Figure 4 and Figure S3). As shown in Figure 4, the band gap of ZnO is reduced from 2.20 to 1.95 eV through the substitutional nitrogen doping, and the contribution of nitrogen to the top of the valence band (VB) of ZnO plays the major role of extending the absorption of N-ZnO to the visible region.

The morphologies of the as-prepared samples were then investigated with scanning electron microscopy (SEM) and transmission electron microscopy (TEM). Figure 5 shows that the ZnOHF sample is composed of agglomerated nanobelts with diameters of 300−400 nm and lengths of up to micrometers. After heating the ZnOHF precursor in NH_3 at temperatures lower than 973 K, the as-prepared N-ZnO powder preserved the original morphology of the nanobelts and the nanobelts were agglomerated into nanobundles. However, the dimensions of the nanobelts and the corresponding nanobundles became smaller with the increase of the heating temperature. Moreover, high-magnification SEM indicated that the nanobelts were composed of agglomerated nanoparticles with diameter of less than 100 nm. The TEM images again confirmed that the nanobelt was composed of agglomerated

dx.doi.org/10.1021/jp311729b | J. Phys. Chem. C 2013, 117, 4937−4942

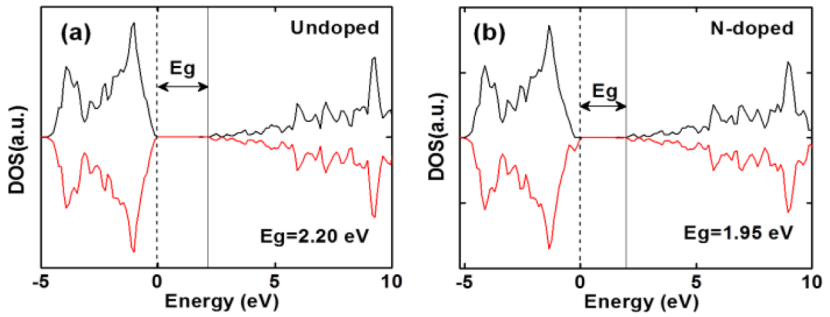

Figure 4. Calculated density of states. Black and red lines are spin-up and spin-down: (a) undoped ZnO, (b) N-doped ZnO. The Fermi level has been shifted to the top of valence band, indicated by the dashed line. The bottom of conduction band is indicated by the straight line.

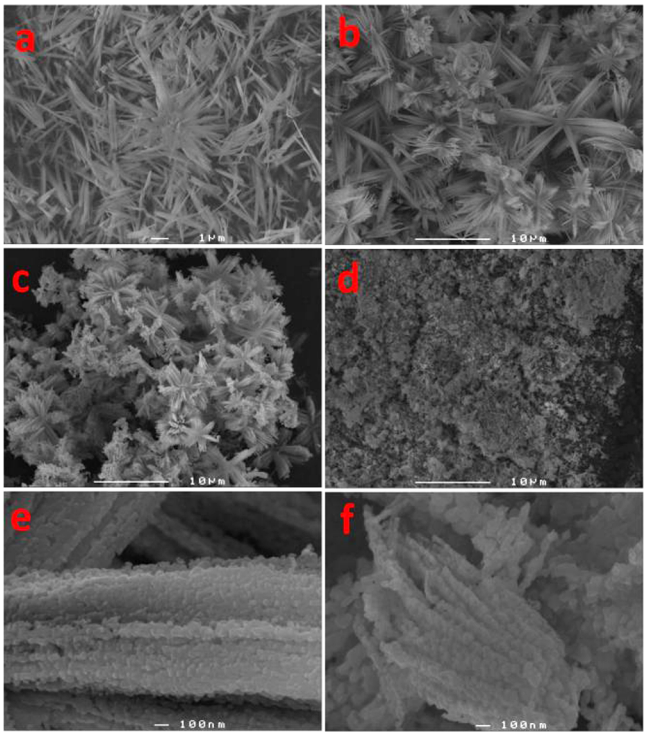

Figure 5. SEM images of (a) ZnOHF precursor and N-ZnO prepared by heating ZnOHF in NH_3 at (b, e) 873 K, (c) 973 K, and (d, f) 1073 K for 2 h.

nanoparticles and elemental mapping analysis indicated that Zn, O, and N elements are uniformly distributed among the bundle-like nanoparticles (Figure 6). During the nitridation synthesis, ZnO will be partially reduced to Zn in a highly reductive atmosphere, and the resulting Zn will vaporize due to its low melting point.[5] Therefore, it is reasonable to suppose that the decreased dimension of the nanobundles is ascribed to the gradual loss of its constituted elements. When the heating temperature is further increased to 1073 K, due to the more facile reduction of ZnO at higher temperatures, the nanobundle structure was totally destroyed, and only irregular nanoparticles were observed. The collapse of the nanobundle structure is accompanied by the drastic decrease of the crystallinity of N-ZnO (Figure 1), indicating the negative influence of nitridation treatment at excessive temperatures.

3.2. Photocatalytic Activity Measurement. Photocatalytic reactions on the as-prepared powder photocatalysts were then carried out under visible light irradiation (λ > 420 nm). Commercial ZnO did not show any activity for water oxidation under visible light due to its wide band gap. After heating ZnOHF in NH_3, the as-prepared N-ZnO catalysts demonstrated high performance for water oxidation (Figure 7).

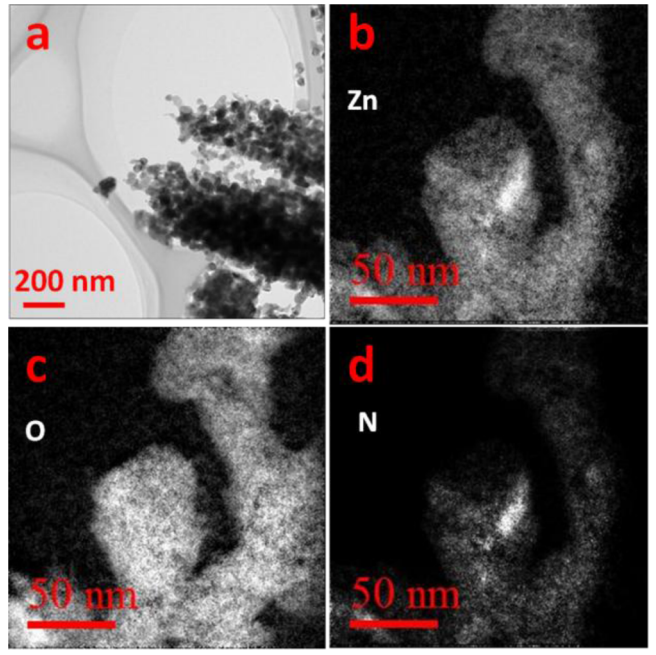

Figure 6. (a) TEM image and (b–d) Zn, O, and N elemental maps for N-ZnO sample prepared at 973 K.

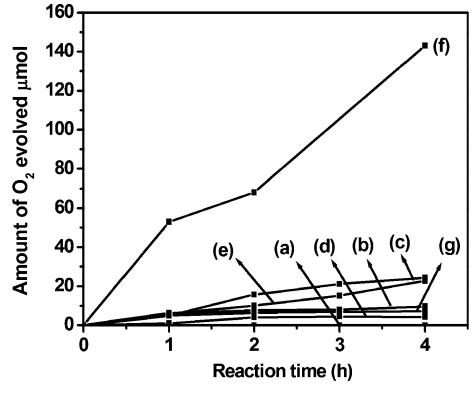

Figure 7. Rates of O_2 evolution on (a) N-doped commercial ZnO, (b–d) N-ZnO prepared by heating ZnOHF precursor in NH_3 gas flow at 873, 973, and 1073 K for 2 h, (e) IrO_2(1 wt %)/commercial N-ZnO, (f) IrO_2(1 wt %)/N-ZnO (N-ZnO was prepared at 973 K), and (g) N-TiO_2.

dx.doi.org/10.1021/jp311729b | J. Phys. Chem. C 2013, 117, 4937–4942

To our knowledge, this is the first report of achieving photocatalytic water oxidation on non-metal-doped ZnO without applied external bias under visible light, therefore extending this important application of ZnO to a wider solar spectrum. It was found that the amount of O_2 evolved on N-ZnO samples prepared at 873, 973, and 1073 K was about 2.4, 5.7, and 1.1 μmol h^{-1}, respectively. As nitridation temperature can play an important role in altering the physicochemical properties of photocatalysts, it will definitely lead to different photocatalytic performance. Similar phenomena have been observed in other well-known nitrides and (oxy)nitride systems such as GaN and GaN-ZnO.[41,42] We also used the commercial N-ZnO as the photocatalyst; however, only a negligible amount of O_2 was detected. From the UV−vis spectra, the N-doped ZnO prepared from the ZnOHF precursor demonstrated drastically enhanced absorption in the visible region compared with N-doped commercial ZnO (Figure 3). This could be one of the main reasons for higher performance of the N-doped ZnO prepared from ZnOHF precursor under visible light irradiation. Because the performance of photocatalyst can be affected by a number of parameters such as surface defects, surface defects, crystallinity, etc., the results presented here can be a reflection of these combined factors, particularly the visible light absorption property. Nevertheless, the present N-ZnO derived from ZnOHF is quite unique in catalyzing water oxidation reactions compared with N-ZnO derived from commercial ZnO. We also tested the photocatalytic activity of N-TiO_2 as a comparison under the same reaction conditions. An average activity of 1.5 μmol h^{-1} was obtained on N-TiO_2, indicating the much higher performance achieved on the present N-ZnO (Figure 7g). It is reported that the performance of photocatalyst can be drastically enhanced by loading proper cocatalyst.[4,6] When IrO_2 nanoparticles were loaded on the surface of N-ZnO, the rate of O_2 evolution on N-ZnO was found to be increased by about 7 times, reaching a rate of 35.8 μmol h^{-1}. Interestingly, O_2 evolution was also observed on IrO_2 loaded commercial N-ZnO, even though the activity is still quite low. Considering that IrO_2 is a highly efficient electrocatalyst for catalyzing O_2 evolution, the loading of IrO_2 on the surface of N-ZnO introduces more active sites for O_2 evolution as a result leading to drastically enhanced photocatalytic activity.

The fact that water oxidation can proceed on the bare N-ZnO nanobundles under visible light inspired us to use this material for photoelectrochemical (PEC) water splitting where external potential was applied. As shown in Figure 8, the photoelectrodes coated with N-ZnO materials exhibited considerable anodic photocurrents upon visible light irradiation, indicating the potential of using the present n-type electrodes for photoelectrochemical water splitting. Moreover, the photocurrent decreased dramatically when N-ZnO photocatalysts prepared at higher temperatures were used as the photoelectrodes. This discrepancy between the photoelectrochemical and photocatalytic performances has also been observed in other systems due to the difference in measurement conditions.[43,44] It is known that the photocorrosion of ZnO is a challenging issue; in this regard, we used $AgNO_3$ as sacrificial reagent. Because the deposition of Ag on N-ZnO surface will decrease the activity of N-ZnO with prolonged reaction time due to the block of light absorption by N-ZnO, it is difficult to study the intrinsic stability N-ZnO at this stage. A detailed investigation of the photoelectrochemical properties of the photoanodes prepared with N-ZnO and their modification with IrO_2 and CoO_x eletrocatalyst is under way.

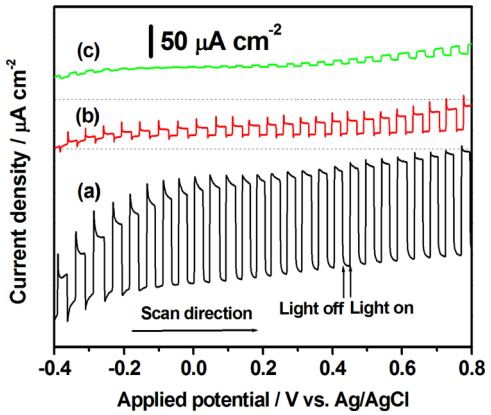

Figure 8. Photoelectrochemical (PEC) water splitting on electrodes coated with N-ZnO nanobundles prepared by calcining ZnOHF precursor in NH_3 gas flow at (a) 873 K, (b) 973 K, and (c) 1073 K for 2 h.

We also tested the photocatalytic activity of N-ZnO for the degradation of organic pollutant. Similar to previous reports, the resultant N-ZnO samples demonstrated quite low activity for the degradation of methylene blue under visible light (data not shown). As the mechanisms for water oxidation and pollutant degradation are different, it is supposed that the surface of N-ZnO possesses active sites for O_2 evolution while lack the reactive sites for pollutant degradation.

4. CONCLUSIONS

In summary, visible-light-responsive N-doped ZnO nanobundles were prepared via a facile nitridation reaction from ZnOHF precursor, which exhibited high photocatalytic performance for water splitting under visible light. The new finding that visible-light-induced water oxidation can be realized on N-ZnO without applied bias will promote the applications of ZnO toward efficient solar energy conversion. Work on optimizing the photocatalytic and photoeletrochemical performance of N-ZnO is underway.

■ ASSOCIATED CONTENT

Supporting Information

XRD, XPS, and theoretical calculation models. This material is available free of charge via the Internet at http://pubs.acs.org.

■ AUTHOR INFORMATION

Corresponding Author

*Fax +61 7 33654199; Tel +61 7 3365218; e-mail l.wang@uq.edu.au.

Notes

The authors declare no competing financial interest.

■ ACKNOWLEDGMENTS

This project was supported by Australian Research Council (through its Centres of Excellence grant and DP programs) and Queensland State Government (NIRAP). We also appreciate the generous grants of CPU time from both the University of Queensland and the Australian National Computational Infrastructure Facility.

REFERENCES

(1) Kudo, A.; Miseki, Y. *Chem. Soc. Rev.* **2009**, *38*, 253.
(2) Liu, G.; Wang, L. Z.; Yang, H. G.; Cheng, H. M.; Lu, G. Q. *J. Mater. Chem.* **2010**, *20*, 831.
(3) Zong, X.; Xing, Z.; Yu, H.; Chen, Z. G.; Tang, F. Q.; Zou, J.; Lu, G. Q.; Wang, L. Z. *Chem. Commun.* **2011**, *47*, 11742.
(4) Mukherji, A.; Seger, B.; Lu, G. Q.; Wang, L. Z. *ACS Nano* **2011**, *5*, 3483.
(5) Maeda, K.; Teramura, K.; Lu, D.; Takata, T.; Saito, N.; Inoue, Y.; Domen, K. *Nature* **2006**, *440*, 295.
(6) Zong, X.; Yan, H.; Wu, G.; Ma, G.; Wen, F.; Wang, L.; Li, C. *J. Am. Chem. Soc.* **2008**, *130*, 7176.
(7) Daneshvar, N.; Salari, D.; Khataee, A. R. *J. Photochem. Photobiol., A* **2004**, *162*, 317.
(8) Khodja, A. A.; Sehili, T.; Pilichowski, J. F.; Boule, P. *J. Photochem. Photobiol., A* **2001**, *141*, 231.
(9) Morrison, S. R.; Freund, T. *J. Chem. Phys.* **1967**, *47*, 1543.
(10) Chen, Z. G.; Ni, A. Z.; Li, F.; Cong, H. t.; Cheng, H. M.; Lu, G. Q. *Chem. Phys. Lett.* **2007**, *434*, 301.
(11) Mapa, M.; Gopinath, C. S. *Chem. Mater.* **2009**, *21*, 351.
(12) Asahi, R.; Morikawa, T.; Ohwaki, T.; Aoki, K.; Taga, Y. *Science* **2001**, *293*, 269.
(13) Anpo, M. *Pure Appl. Chem.* **2000**, *72*, 1265.
(14) Liu, W.; Gu, S. L.; Ye, J. D.; Zhu, S. M.; Wu, Y. X.; Shan, Z. P.; Zhang, R.; Zheng, Y. D.; Choy, S. F.; Lo, G. Q.; Sun, X. W. *J. Cryst. Growth* **2008**, *310*, 3448.
(15) Cao, P.; Zhao, D. X.; Zhang, J. Y.; Shen, D. Z.; Lu, Y. M.; Yao, B.; Li, B. H.; Bai, Y.; Fan, X. W. *Appl. Surf. Sci.* **2008**, *254*, 2900.
(16) Liu, W. W.; Yao, B.; Zhang, Z. Z.; Li, Y. F.; Li, B. H.; Shan, C. X.; Zhang, J. Y.; Shen, D. Z.; Fan, X. W. *J. Appl. Phys.* **2011**, *109*, 093518.
(17) Erdogan, N. H.; Kara, K.; Ozdamar, H.; Kavak, H.; Esen, R.; Karaagac, H. *J. Alloys Compd.* **2011**, *509*, 8922.
(18) Zhao, J. L.; Li, X. M.; Bian, J. M.; Yu, W. D.; Zhang, C. Y. *J. Cryst. Growth* **2005**, *280*, 495.
(19) Lin, H. F.; Liao, S. C.; Hung, S. W. *J. Photochem. Photobiol., A* **2005**, *174*, 82.
(20) Uekawa, N.; Kojima, T.; Kakegawa, K. *J. Mater. Res.* **2009**, *24*, 3343.
(21) Zheng, M.; Wu, J. Q. *Appl. Surf. Sci.* **2009**, *255*, 5656.
(22) Peng, Y. *Chin. J. Chem.* **2011**, *29*, 191.
(23) Kohn, W.; Sham, L. J. *Phys. Rev.* **1965**, *140*, 1133.
(24) Perdew, J. P.; Burke, K.; Ernzerhof, M. *Phys. Rev. Lett.* **1996**, *77*, 3865.
(25) Kresse, G.; Joubert, D. *Phys. Rev. B* **1999**, *59*, 1758.
(26) Kresse, G.; Furthmuller, J. *Phys. Rev. B* **1996**, *54*, 11169.
(27) Kresse, G.; Furthmuller, J. *Comput. Mater. Sci.* **1996**, *6*, 15.
(28) Anisimov, V. I.; Zaanen, J.; Andersen, O. K. *Phys. Rev. B* **1991**, *44*, 943.
(29) Pacchioni, G. *J. Chem. Phys.* **2008**, *128*, 182505.
(30) Vladimir, I. A.; Aryasetiawan, F.; Lichtenstein, A. I. *J. Phys.: Condens. Matter* **1997**, *9*, 767.
(31) Palacios, P.; Aguilera, I.; Wahnon, P. *Thin Solid Films* **2010**, *518*, 4568.
(32) Zhou, G. C.; Sun, L. Z.; Zhong, X. L.; Chen, X.; Wei, L.; Wang, J. B. *Phys. Lett. A* **2007**, *368*, 112.
(33) Paudel, T. R.; Lambrecht, W. R. L. *Phys. Rev. B* **2008**, *77*, 205202.
(34) Li, Q. W.; Bian, J. M.; Sun, J. C.; Liang, H. W.; Zou, C. W.; Sun, Y. L.; Luo, Y. M. *Appl. Surf. Sci.* **2010**, *257*, 1634.
(35) Vijayaraj, M.; Gopinath, C. S. *J. Catal.* **2006**, *241*, 83.
(36) Musat, V.; Rego, A. M.; Monteiro, R.; Fortunato, E. *Thin Solid Films* **2008**, *516*, 1512.
(37) Toyoura, K.; Tsujimura, H.; Goto, T.; Hachiya, K.; Hagiwara, R.; Ito, Y. *Thin Solid Films* **2005**, *492*, 88.
(38) Perkins, C. L.; Lee, S. H.; Li, X. N.; Asher, S. E.; Coutts, T. J. *J. Appl. Phys.* **2005**, *97*, 034907.
(39) Bian, J. M.; Li, X. M.; Gao, X. D.; Yu, W. D.; Chen, L. D. *Appl. Phys. Lett.* **2004**, *84*, 541.
(40) Huang, Q. L.; Wang, M.; Zhong, H. X.; Chen, X. T.; Xue, Z. L.; You, X. Z. *Cryst. Growth Des.* **2008**, *8*, 1412.
(41) Maeda, K.; Saito, N.; Inoue, Y.; Domen, K. *Chem. Mater.* **2007**, *19*, 4092.
(42) Maeda, K.; Teramura, K.; Takata, T.; Hara, M.; Saito, N.; Toda, K.; Inoue, Y.; Kobayashi, H.; Domen, K. *J. Phys. Chem. B* **2005**, *109*, 20504.
(43) Iwashina, K.; Kudo, A. *J. Am. Chem. Soc.* **2011**, *133*, 13272.
(44) Hashiguchi, H.; Maeda, K.; Abe, R.; Ishikawa, A.; Kubota, J.; Domen, K. *Bull. Chem. Soc. Jpn.* **2009**, *82*, 401.